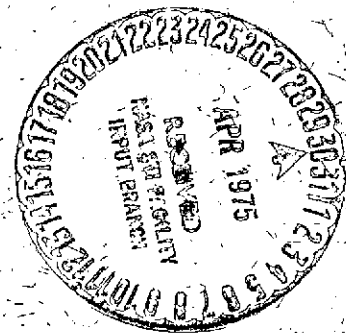# MICROWAVE EMISSION FROM SNOW AND GLACIER ICE

T. C. CHANG
P. GLOERSEN
T. SCHMUGGE
T. T. WILHEIT
H. J. ZWALLY

FEBRUARY 1975

For information concerning availability
of this document contact:

Technical Information Division, Code 250
Goddard Space Flight Center
Greenbelt, Maryland 20771

(Telephone 301–982–4488)

MICROWAVE EMISSION FROM SNOW AND GLACIER ICE

T. C. Chang
P. Gloersen
T. Schmugge
T. T. Wilheit
H. J. Zwally

CONTENTS

TABLES

ILLUSTRATIONS

ILLUSTRATIONS (Cont'd)

MICROWAVE EMISSION FROM SNOW AND GLACIER ICE

I. INTRODUCTION

Recent observations using the Electrically Scanned Microwave Radiometer (ESMR) on board the NIMBUS-5 satellite over the continental ice sheets of Greenland and Antarctica (Gloersen et al., 1974) have been puzzling in that there is a complete lack of correlation between microwave brightness temperature and physical surface temperature in Greenland, whereas in Antarctica there is a loose correlation over wide areas. This has provided additional incentive for developing an applicable analytical model for explaining the microwave emission from snow and glacier ice. In addition, other experimental observations made on board aircraft sensor platforms over smaller glaciers, snow fields, and sea ice have been difficult to interpret in terms of existing models.

A useful insight into the microwave emission from snow fields has been provided by a macroscopic volume scattering model (England, 1974), which was also developed for other solid dielectrics such as moist soil. England's treatment involves specifically a parameter called the volume scattering albedo, ω_0, which is the ratio of the volume scattering coefficient to the total extinction coefficient. The extinction coefficient includes both the resistive losses and the scattering. The analysis involves specifying a value for ω_0 and then computing the brightness temperature or emissivity based on this single parameter. The model may be used to calculate the emissivity or the brightness temperature of finite slabs of snow and ice with varying composition.

In this paper, a microscopic approach will be taken in which it is assumed that the snow field or snow cover consists of closely packed scattering spheres which do not interact coherently. These assumptions then permit the utilization of the Mie scattering theory (Stratton, 1941) in computing ω_0 and its several components. The treatment is similar in many respects to that used in calculating microwave and optical properties of clouds (Gaut and Reifenstein 1971, Curran et al., 1975). One important similarity is that the particle size is comparable to the wavelength of the microwave radiation within the particle in both cases, since the particle sizes encountered in snow fields are sufficiently larger than cloud droplets to compensate for the lower index of refraction of the ice particles. An important difference in detail of this treatment is that the imaginary part of the dielectric constant of ice is orders of magnitude smaller than for water droplets, grossly reducing the absorption cross-section of the particle.

Since the Mie scattering model provides many more reflecting surfaces than any reasonable multilayer (resulting from seasonal snow accumulations) model or variable dielectric model would provide, it dominates the contribution to the

1

volume extinction coefficient at the microwave wavelengths and for subsurface snow particle sizes encountered. It will be shown that the penetration depths vary from 10 to 100 wavelengths depending on the snow and ice conditions encountered. Thus, the effects of snow cover dominate in most observations of snow-covered glaciers at the wavelength of 1.55 cm used in the NIMBUS-5 ESMR.

II. ANALYTICAL APPROACH

It shall be assumed that the snow and ice fields of interest consist mostly of spherical particles of water ice, with various values of the loss tangent at a given microwave wavelength. The exact theoretical study of the electromagnetic wave scattering by spherical particles was done by Mie (1908). By utilizing the Mie theory, the extinction and scattering cross-sections of spherical ice particles can be calculated for all ranges of particle size and radiation wavelengths as a function of both the particle radius r and the complex index of refraction n.

The extinction cross-section σ_{EXT}, scattering cross-section σ_{SCA} and absorption cross-section σ_{ABS} for particles of radius r and the complex index of refraction n can be written as:

$$\sigma_{EXT} = \frac{\lambda^2}{2\pi} \sum_{m=1}^{\infty} (2m + 1)(-1) \, \text{Re} \, [a_m + b_m] \tag{1}$$

$$\sigma_{SCA} = \frac{\lambda^2}{2\pi} \sum_{m=0}^{\infty} (2m + 1)\,[\,|a_m|^2 + |b_m|^2\,] \tag{2}$$

and

$$\sigma_{ABS} = \sigma_{EXT} - \sigma_{SCA} \tag{3}$$

where a_m and b_m are the complex Mie scattering coefficients which contain Bessel and Neumann functions of 1/2 integer order. That is,

$$a_m = \frac{\left[\dfrac{A_m}{n} + \dfrac{m\lambda}{2\pi r}\right] J_{m+\frac{1}{2}}\left(\dfrac{2\pi r}{\lambda}\right) - J_{m-\frac{1}{2}}\left(\dfrac{2\pi r}{\lambda}\right)}{\left[\dfrac{A_m}{n} + \dfrac{m\lambda}{2\pi r}\right]\left[J_{m+\frac{1}{2}}\left(\dfrac{2\pi r}{\lambda}\right) + i(-1)^m J_{-m-\frac{1}{2}}\left(\dfrac{2\pi r}{\lambda}\right)\right] - J_{m-\frac{1}{2}}\left(\dfrac{2\pi r}{\lambda}\right) + i(-1)^m J_{-m+\frac{1}{2}}\left(\dfrac{2\pi r}{\lambda}\right)} \qquad (4)$$

$$b_m = \frac{\left[A_m n + \dfrac{m\lambda}{2\pi r}\right] J_{m+\frac{1}{2}}\left(\dfrac{2\pi r}{\lambda}\right) - J_{m-\frac{1}{2}}\left(\dfrac{2\pi r}{\lambda}\right)}{\left[A_m n + \dfrac{m\lambda}{2\pi r}\right]\left[J_{m+\frac{1}{2}}\left(\dfrac{2\pi r}{\lambda}\right) + i(-1)^m J_{-m-\frac{1}{2}}\left(\dfrac{2\pi r}{\lambda}\right)\right] - J_{m-\frac{1}{2}}\left(\dfrac{2\pi r}{\lambda}\right) + i(-1)^m J_{-m+\frac{1}{2}}\left(\dfrac{2\pi r}{\lambda}\right)} \qquad (5)$$

$$A_m = -\frac{m\lambda}{2\pi r n} + \left[\frac{J_{m-\frac{1}{2}}\left(\dfrac{2\pi r n}{\lambda}\right)}{J_{m+\frac{1}{2}}\left(\dfrac{2\pi r n}{\lambda}\right)}\right] \qquad (6)$$

where λ is the free space wavelength, r is the particle radius, n is the complex index of refraction, J_m denotes a Bessel function of order m and J_{-m} denotes the corresponding Neumann function. The extinction cross-section for spherical ice particles with refractive index $n = 1.78 + i\ 0.0024$, which corresponds to measured values in the cm wavelength range of pure water ice near its melting point (Cumming, 1952), is calculated for several wavelengths and particle sizes. The results of the calculations in terms of the extinction coefficient (see Equations (8) and (15)), are shown in Figure 1. By using this relatively high value of Im(n), the importance of the scattering contribution to the extinction cross-section is emphasized, since it dominates even at this value of Im(n). The computation serves to illustrate the dependence of volume scattering on particle sizes in this wavelength range.

Although the added complexity of calculating for various temperatures, snow density, and crystal size profiles is well within the capability of the computational technique, a simplified model is constructed for the purpose of illustration. A layer of uniformly sized spheres (the snow cover) of complex index n is situated on top of a perfectly absorbing medium (the glacier ice). The physical temperature in the snow layer is assumed to be uniform and at 250° K for simplicity. The actual temperature of the underlying glacier ice, assumed to be 270° K, will be important only for very thin snow covers. Since the change in the dielectric constant from the ice to air would give less than 10% reflectivity and since the presence of the snow layer above both mitigates this abrupt dielectric change and introduces opacity between the ice and radiatively cold outer space, this model is reasonable except in the limit of vanishing snow

3
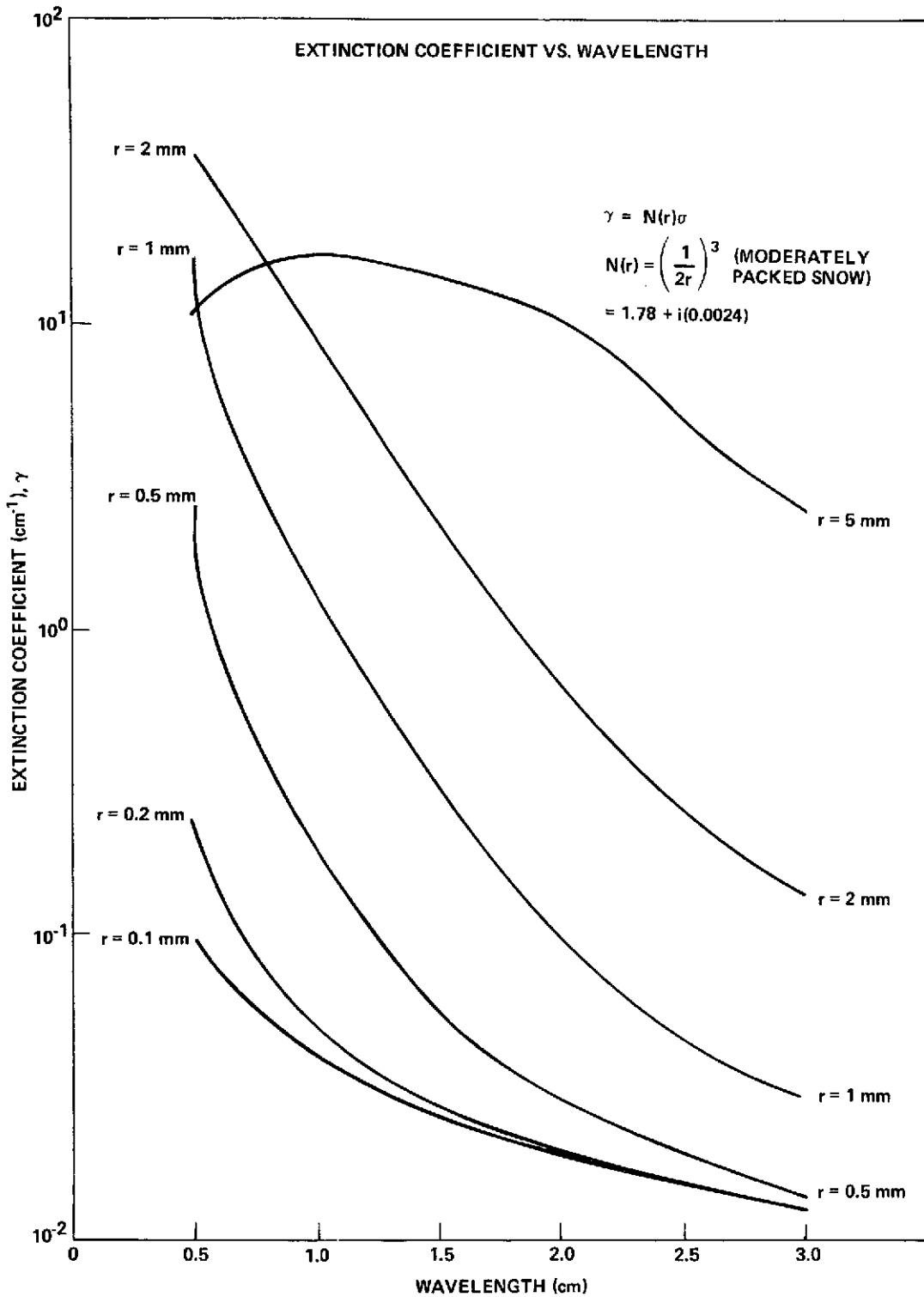
Figure 1. Extinction coefficient as a function of microwave wavelength for several ice crystal radii

thickness. The model is illustrated in Figure 2. Since the snow layer is assumed to be a temperature of 250°K, the appropriate index of refraction is n = 1.78 + i 0.0005 (Cumming, 1952). An additional simplification is that only the radiation emanating normal to the surface will be calculated. In this case, the distinction between the two polarizations breaks down due to symmetry. Also, the ice particles are assumed to be randomly distributed and the interaction between ice particles is not dependent on the path length.
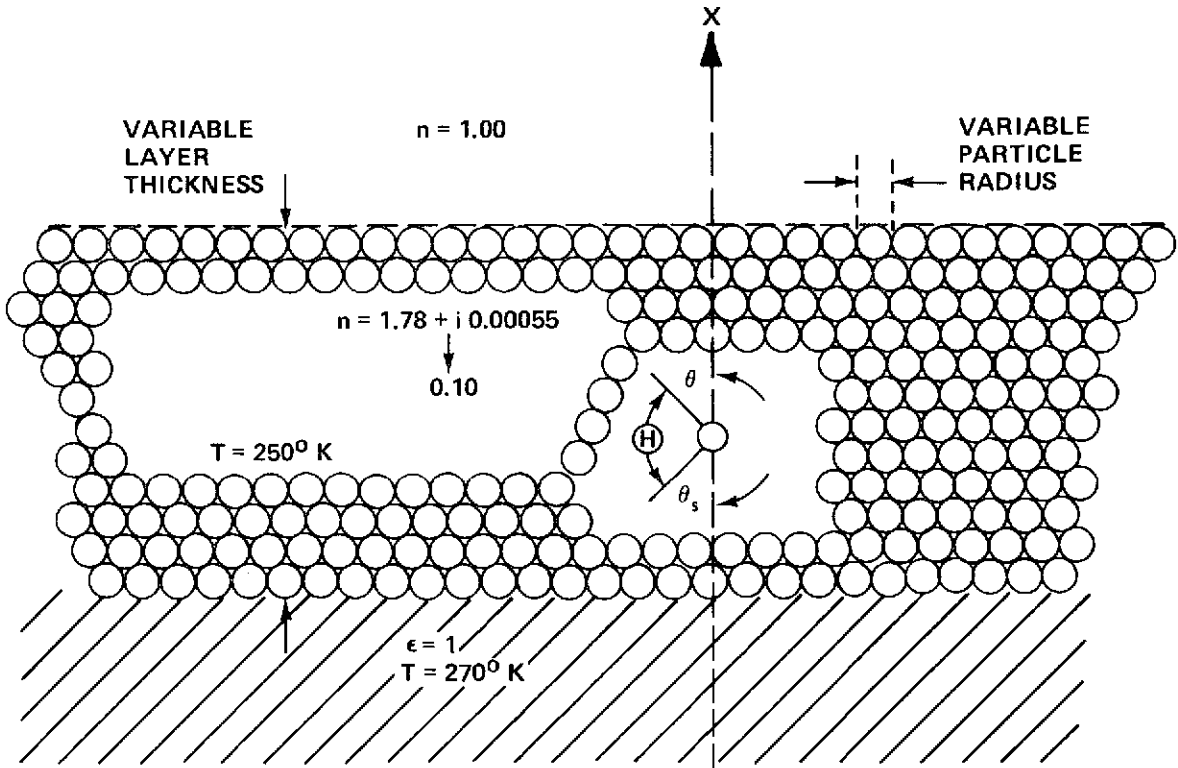
Figure 2. Sketch of the single layer scattering model

The Rayleigh-Jeans approximation for the intensity of thermal radiation from a blackbody is applicable at microwave frequencies and at temperatures typical of the earth and its atmosphere; thus the radiative transfer equation (Chandrasekhar, 1950) with axial symmetry, may be written as:

$$\frac{d T_B (\theta)}{d X} + \gamma_{EXT} T_B (\theta) = \frac{\gamma_{SCA}}{2} \int_0^{2\pi} T_B (\theta_s) F(\theta, \theta_s) \, Sin \, \theta_s d\theta_s + \gamma_{ABS} T(X) \qquad (7)$$

5

where $T_B(\theta)$ is radiance in the direction (θ) expressed as equivalent blackbody temperature, $T(X)$ is the thermodynamic temperature of the absorbing medium, and γ_{EXT}, γ_{SCA}, and γ_{ABS} are the extinction, the scattering, and the absorption coefficients respectively, defined as

$$\gamma_i = N\sigma_i \tag{8}$$

where N is the number of particles per unit volume. $F(\theta, \theta_s)$ is the scattering phase function which is defined as the fraction of incident energy scattered into unit solid angle about a direction which makes an angle $(\widehat{H})$ with the θ and θ_s:

$$F(\theta, \theta_s) = \frac{\lambda^2}{8\pi^2} \left\{ |S_1((\widehat{H}))|^2 + |S_2((\widehat{H}))|^2 \right\} \tag{9}$$

where $S_1((\widehat{H}))$ and $S_2((\widehat{H}))$ are scattering amplitude functions

$$S_1((\widehat{H})) = \sum_{m=1}^{\infty} \frac{2m+1}{m(m+1)} \left\{ a_m \Pi_m + b_m \tau_m \right\} \tag{10}$$

$$S_2((\widehat{H})) = \sum_{m=1}^{\infty} \frac{2m+1}{m(m+1)} \left\{ b_m \Pi_m + a_m \tau_m \right\} \tag{11}$$

a_m and b_m are the same as defined in equations (4) and (5); Π_m and τ_m are functions of Legendre polynomials

$$\Pi_m = P_m (\cos \theta) \tag{12}$$

$$\tau_m = \cos \theta \, \Pi_m - \sin^2 \theta \, \frac{d}{d \cos \theta} (\Pi_m) \tag{13}$$

6

Equation (7) is solved numerically by first noting that it may be expressed as:

$$\frac{dT_B(\theta)}{dX} + \gamma_{ABS}(T_B(\theta) - T(X)) = \frac{\gamma_{SCA}}{2} \int_0^{2\pi} T_B(\theta_s) F(\theta, \theta_s) \sin \theta_s d\theta_s - \gamma_{SCA} T_B(\theta) \qquad (14)$$

For a non-scattering medium, the left-hand side of the equation would be equated to zero; the right-hand side represents the angular distribution of radiation resulting from the scattering. To solve this equation, the snow layer is first divided into a number of smaller layers. An initial estimate is then made of the brightness temperature as a function of angle in each of these layers, insuring that the top and bottom layers obey the appropriate boundary conditions, namely, that the downwelling radiation is zero in the top layer and that the upwelling brightness temperature is 270° K in the bottom layer. The downwelling brightness temperature can then be calculated from the top layer downward using the estimated brightness for the scattering terms. The upwelling components are then similarly calculated from the bottom up. The process is repeated maintaining the boundary conditions until a satisfactory convergence is obtained, for which five passes was sufficient for all cases in this study. The method of solution is a variation of the Gauss-Seidal iteration (Hildebrande, 1946).

III. COMPUTATIONAL RESULTS

Using the formalism developed in the preceding section, a set of brightness temperatures are calculated for wavelengths of 2.81, 1.55, and 0.81 cm with ice particle layer thicknesses from 10 cm to 20 m and with particle radii ranging from 0.1 mm to 5 mm. The variation in the particle density, N(r) for different particle sizes is described as follows:

$$N(r) = \left(\frac{1}{2r}\right)^3 \qquad (15)$$

This corresponds to mass densities typical of moderately packed snow (450 Kg m^{-3}). The calculated brightness temperatures are displayed in Figures 3, 4 and 5. In these figures, an asymptotic behavior is apparent when the thickness of the spherical particle layer becomes large compared with the wavelength, implying that little radiation emanates from depths greater than the penetration depth defined by such thickness. For the particle with radius 0.2 mm, typical of

7

Figure 3. Brightness temperature as a function of ice crystal radius for several values of the single layer depth and for a microwave wavelength of 2.81 cm

BRIGHTNESS TEMPERATURE vs ICE CRYSTAL RADIUS

λ =1.55cm

N = 1.78 + i 0.00055

20 m

10 m

5 m

2 m

1 m

10 cm

20 cm

50 cm

BRIGHTNESS TEMPERATURE (°K)

RADIUS mm

Figure 4. Brightness temperature as a function of ice crystal radius for several values of the single layer depth and for a microwave wavelength of 1.55 cm

BRIGHTNESS TEMPERATURE vs ICE CRYSTAL RADIUS

$\lambda = 0.8cm$

10 cm

20 cm

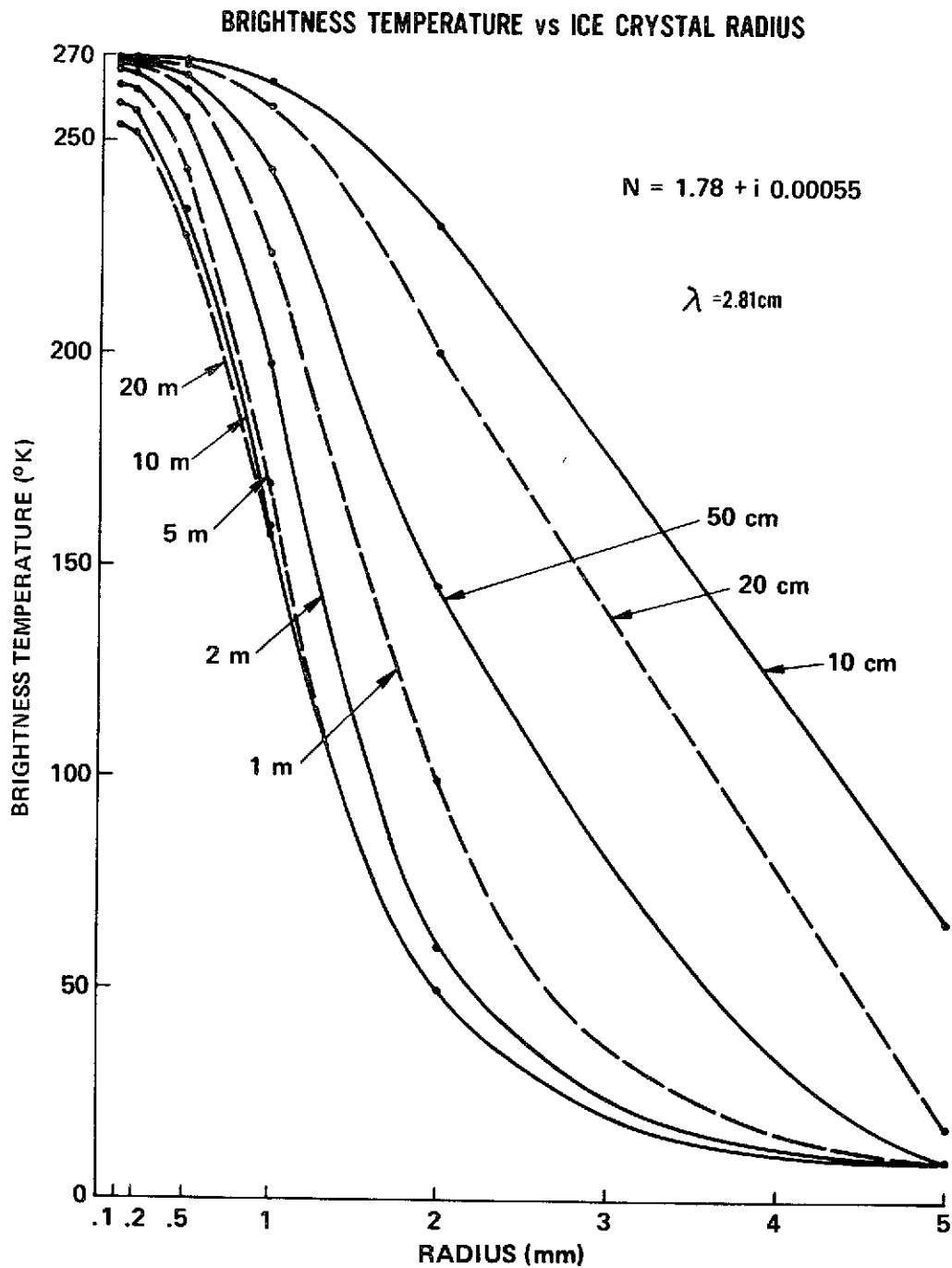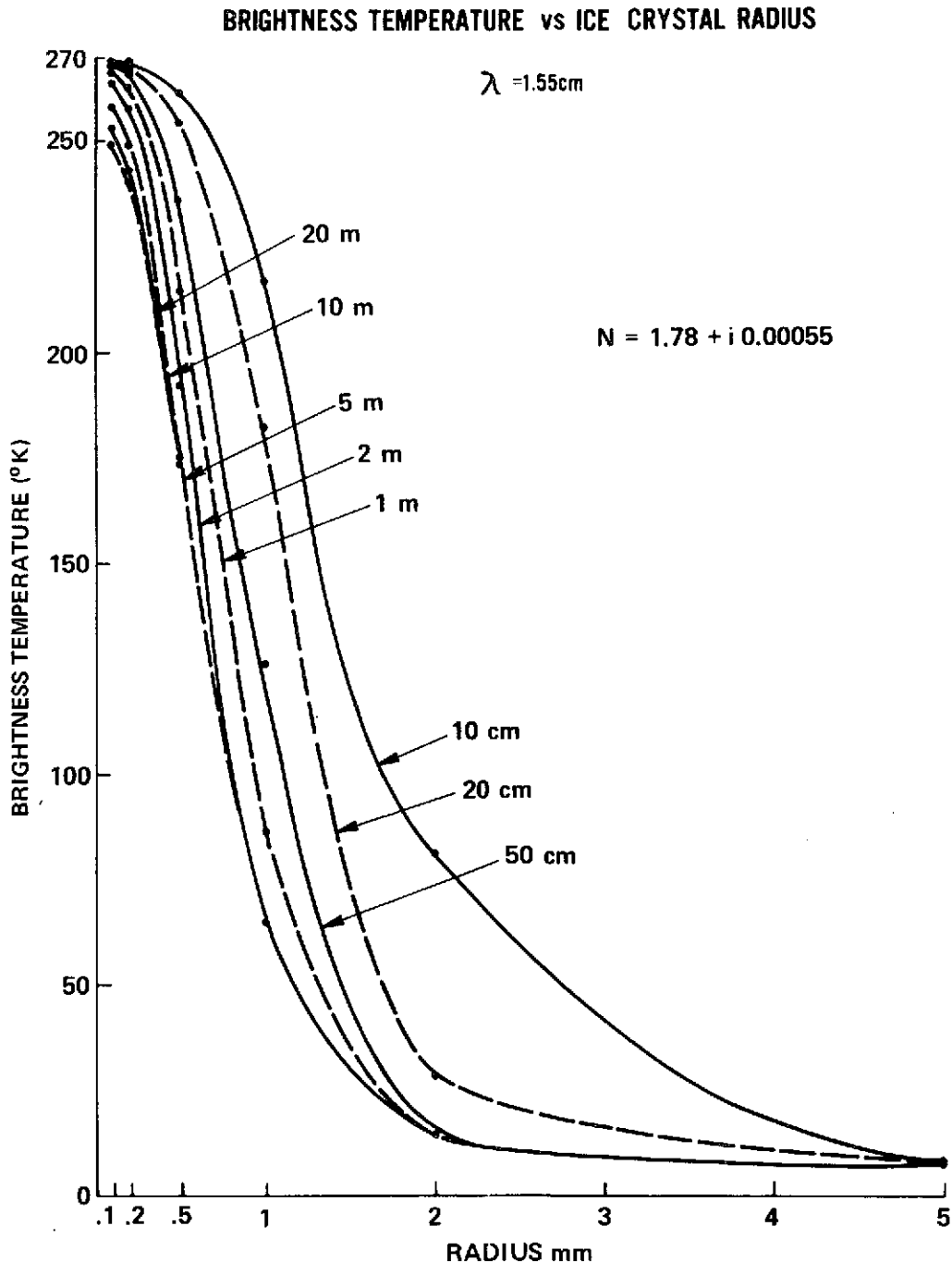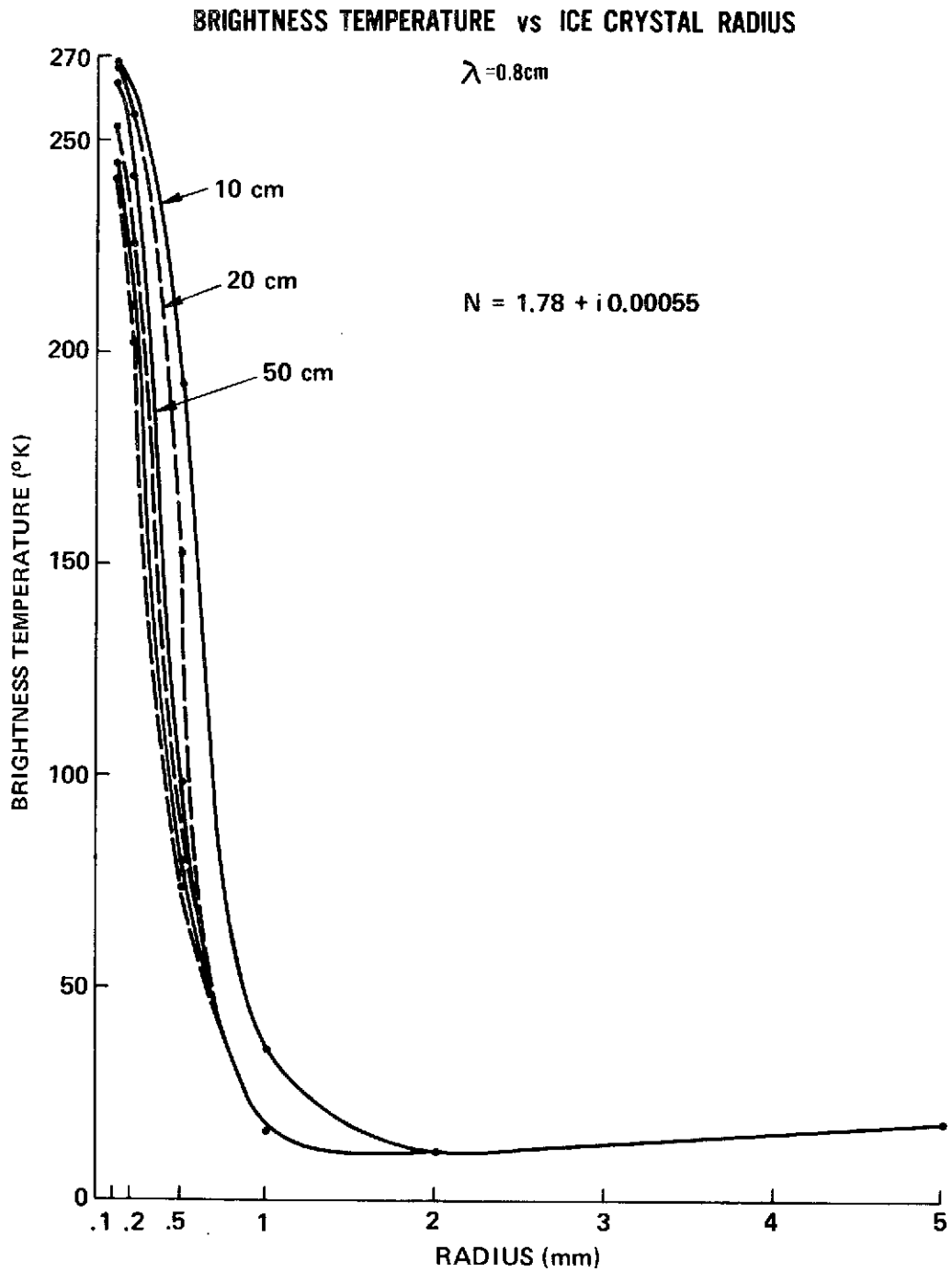$N = 1.78 + i\,0.00055$

50 cm

Figure 5. Brightness temperature as a function of ice crystal radius for several values of the single layer depth and for a microwave wavelength of 0.81 cm

fresh snow, the asymptotic thickness is approximately 10 m for $\lambda = 2.81$ cm, 5 m for $\lambda = 1.55$ cm, and 2 m for $\lambda = 0.8$ cm. The asymptotic value of the brightness temperature of snow layers of increasing thickness depends only upon ω_0, the single scattering albedo in that layer. The asymptotic brightness temperatures calculated for 2.81, 1.55 and 0.81 cm wavelength as a function of ω_0 is plotted in Figure 6.

The consequences of varying the index of refraction in the ice crystals has also been examined. The impurity level in the ice crystals is known to affect the real part of the index only slightly. On the other hand, the imaginary part of the index varies by many orders of magnitude with the introduction of impurities in the 260-273°K temperature range (Hoekstra and Cappillino, 1971). While it is approximately 0.0024 for pure ice near 0°C, it can be as high as 0.1 for first-year sea ice at the same temperature. Such variations are attributed to the lowering of the melting point of the ice and the existence of a two-phase system over a broader temperature range with the presence of metal salts. The variation of the imaginary part of the index of refraction leads to different values of ω_0 for a given wavelength λ and particle radius r. This is illustrated in Figures 7, 8 and 9 for the three wavelength values 2.81, 1.55 and 0.81 cm, respectively. These curves show that ω_0 is a strong function of the loss tangent which, in turn, depends on the physical temperature of the snow. This suggests that in order to determine the ice crystal size by remote sensing, multispectral measurements are needed. Curves such as those shown in Figure 10, in which ω_0 has been eliminated as an intermediate parameter from the curves of Figures 6-9, illustrates this requirement. Determination of the average particle radius from the curves of Figure 10 and from an a priori knowledge of the physical temperature range would be straightforward except for the complicating factors of particle size variation with depth (to be discussed later) and variation of penetration depth with microwave wavelength.

Values of the azimuthally integrated differential scattering cross-section, $F(\theta, \theta_s)$ (see Equation (9)), have been calculated and are shown in dimensionless form in Figure 11. The data are parameterized in terms of the particle size parameter $\alpha \equiv 2\pi r/\lambda$ and are divided by $2\pi\lambda^2$ so that these are valid for all wavelengths. Note that for $\alpha = 0.02$, the forward and backward scattering are essentially equal and the scattering to the side is about half as large. As the particle size increases, the near forward scattering increases much more than the near backward scattering. (Note the curve for $\alpha = 1.12$, Figure 11.) What is more important, however, is that the differential scattering cross-section increases rapidly as α increases, which accounts largely for the behavior of ω_0 as a function of the particle radius (Figures 7-9).

11

Figure 6. Brightness temperature and emissivity as functions of the
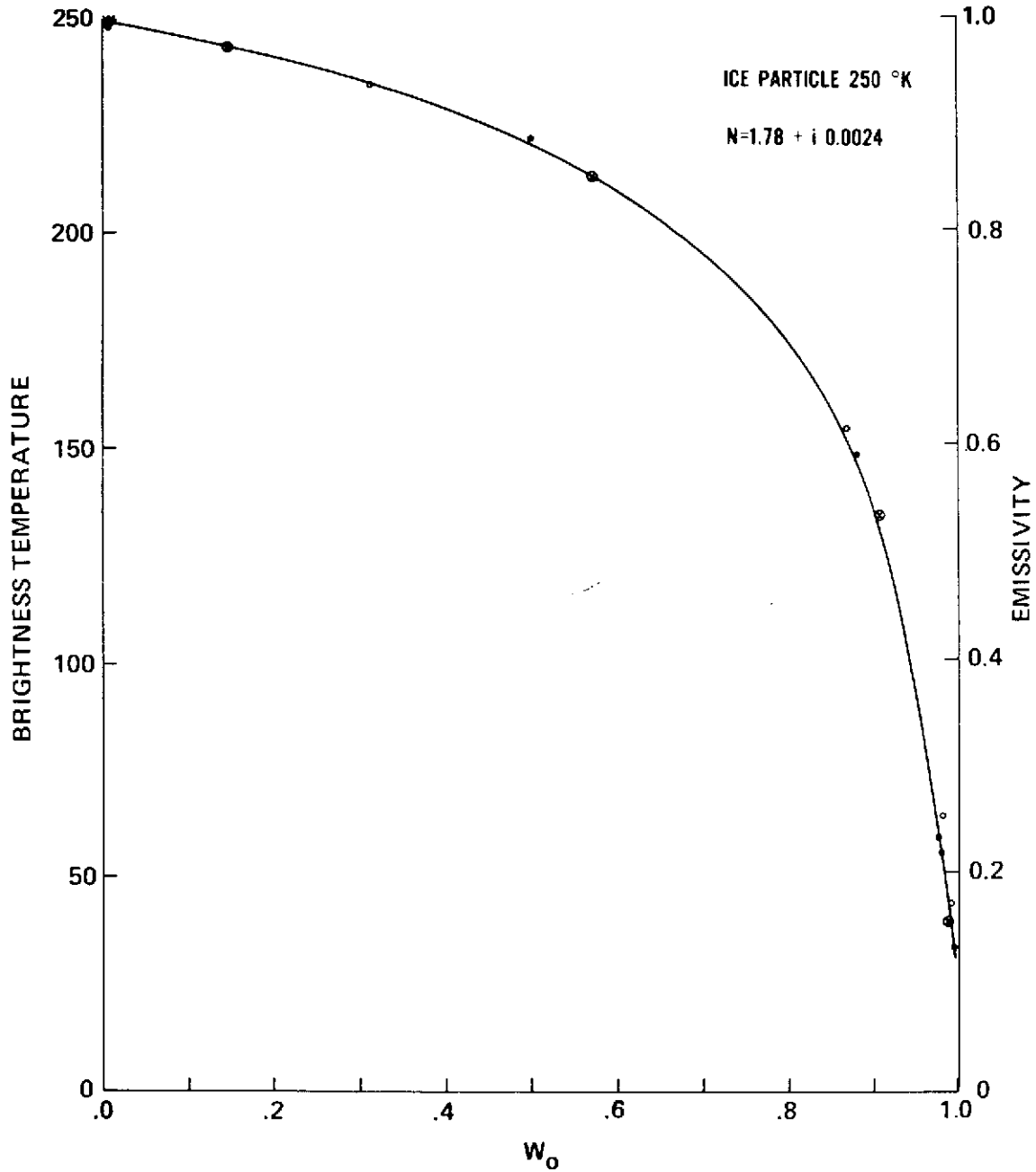volume scattering albedo, $W_0 = \gamma_{SCA} / \gamma_{EXT}$. The values of all
three wavelengths, 2.81 cm (crosses), 1.55 cm (solid circles)
and 0.81 cm (open circles), fall on the same curve.

Figure 7. Volume scattering albedo as a function of ice crystal radius for several values of the imaginary part of the index of refraction and for a wavelength of 2.81 cm

W₀ vs RADIUS (for different losses)

Figure 8. Volume scattering albedo as a function of ice crystal radius for several values of the imaginary part of the index of refraction and for a wavelength of 1. 55 cm
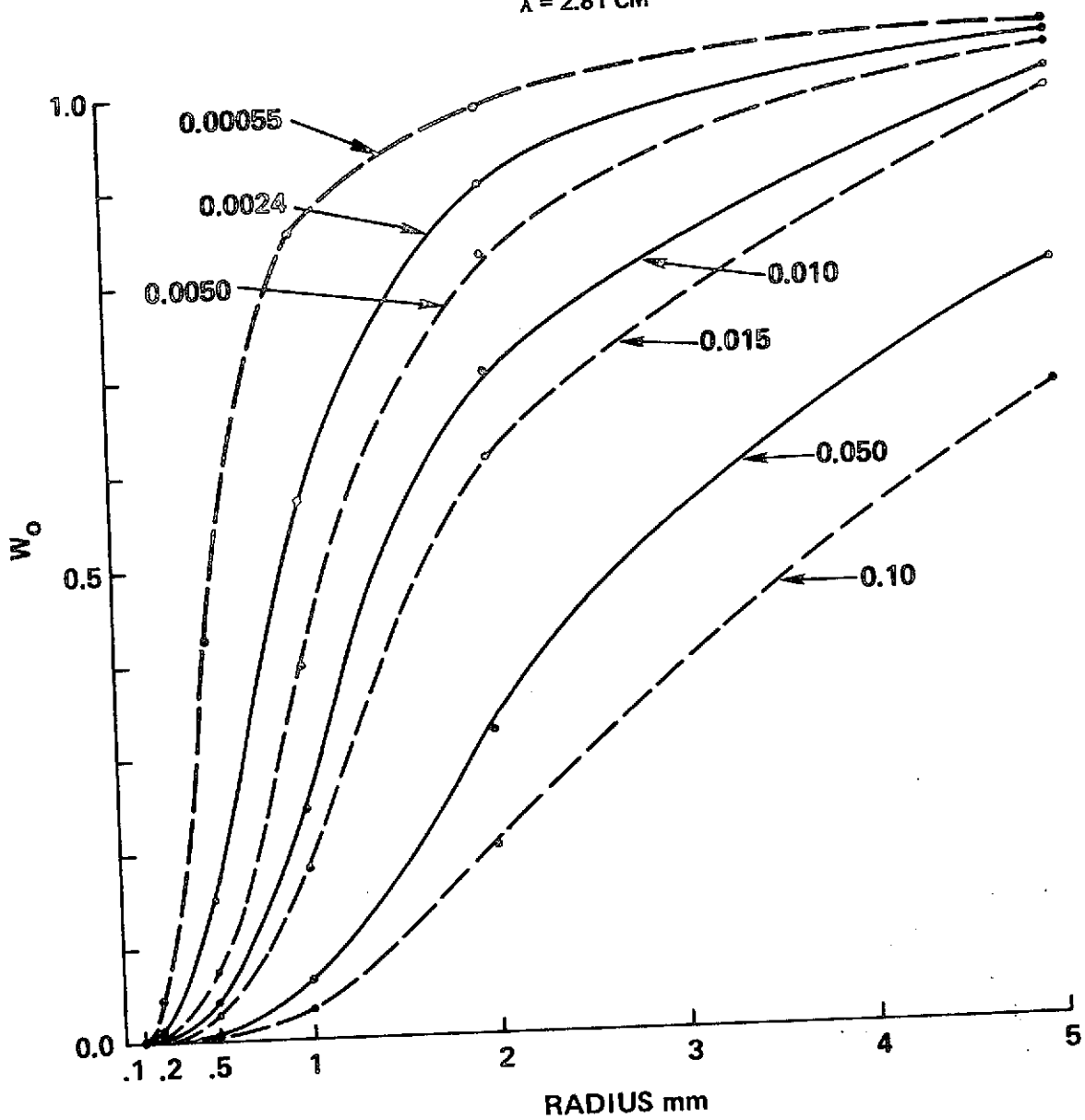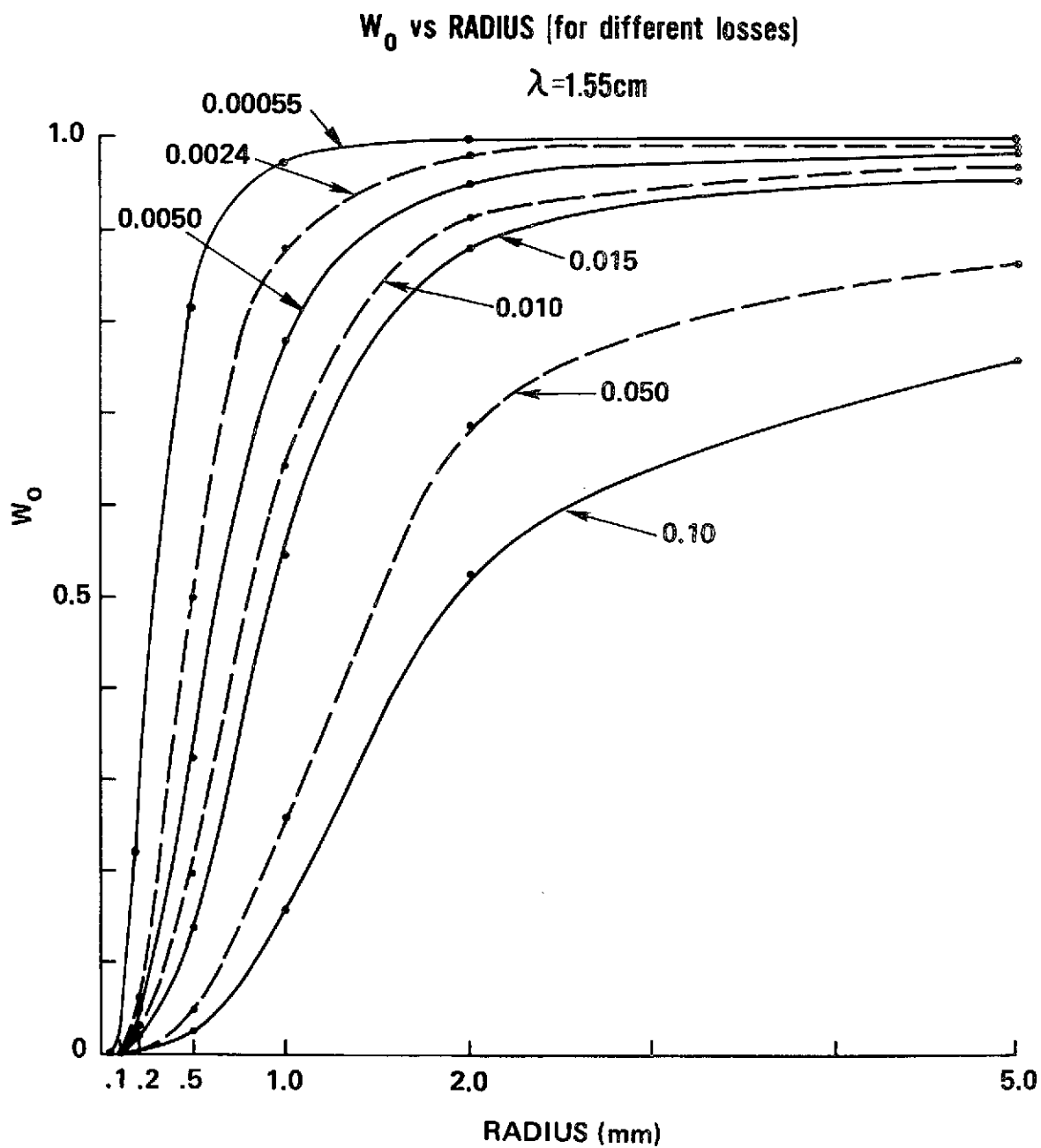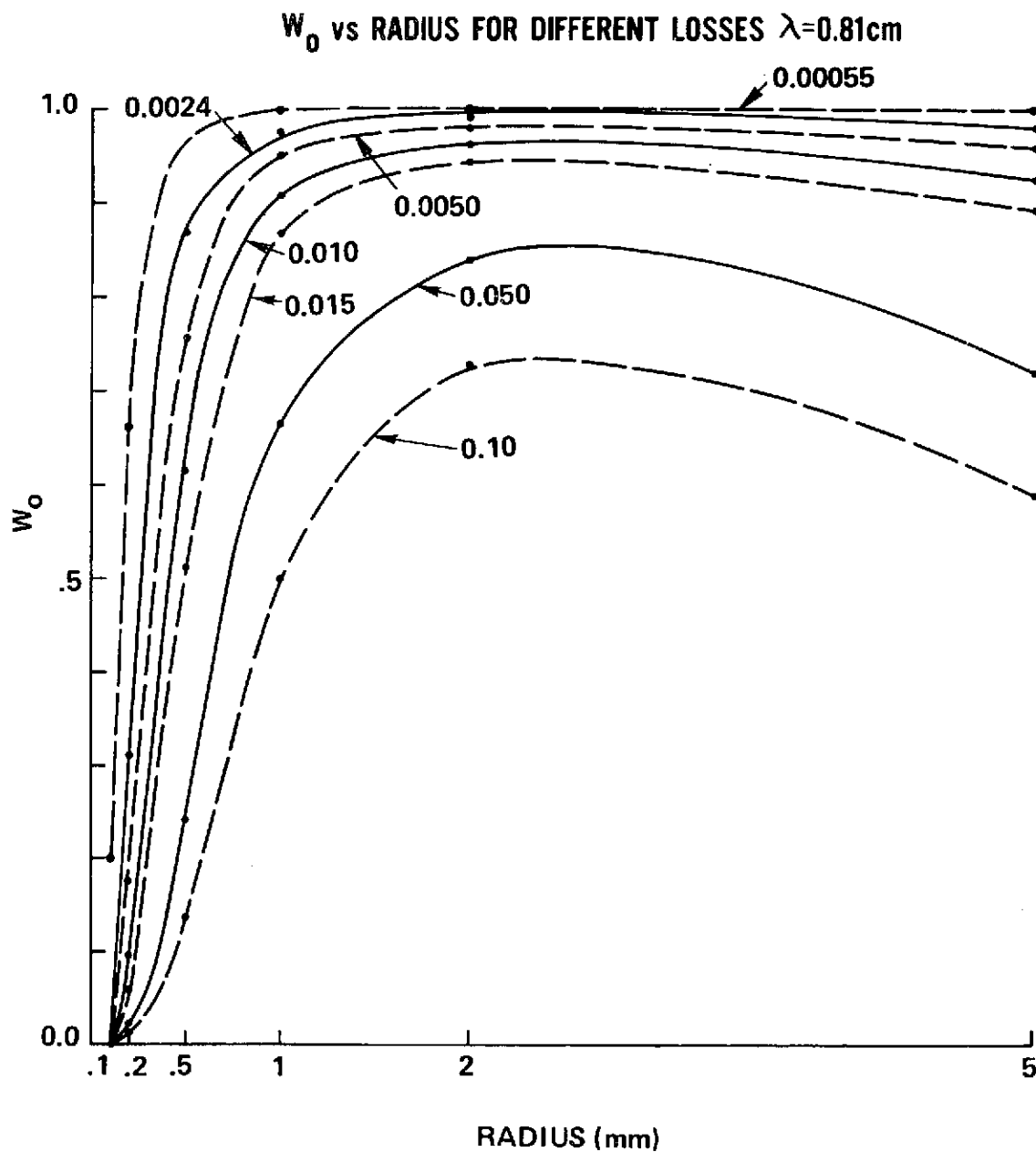
14

Figure 9. Volume scattering albedo as a function of ice crystal radius for several values of the imaginary part of the index of refraction and for a wavelength of 0.81 cm
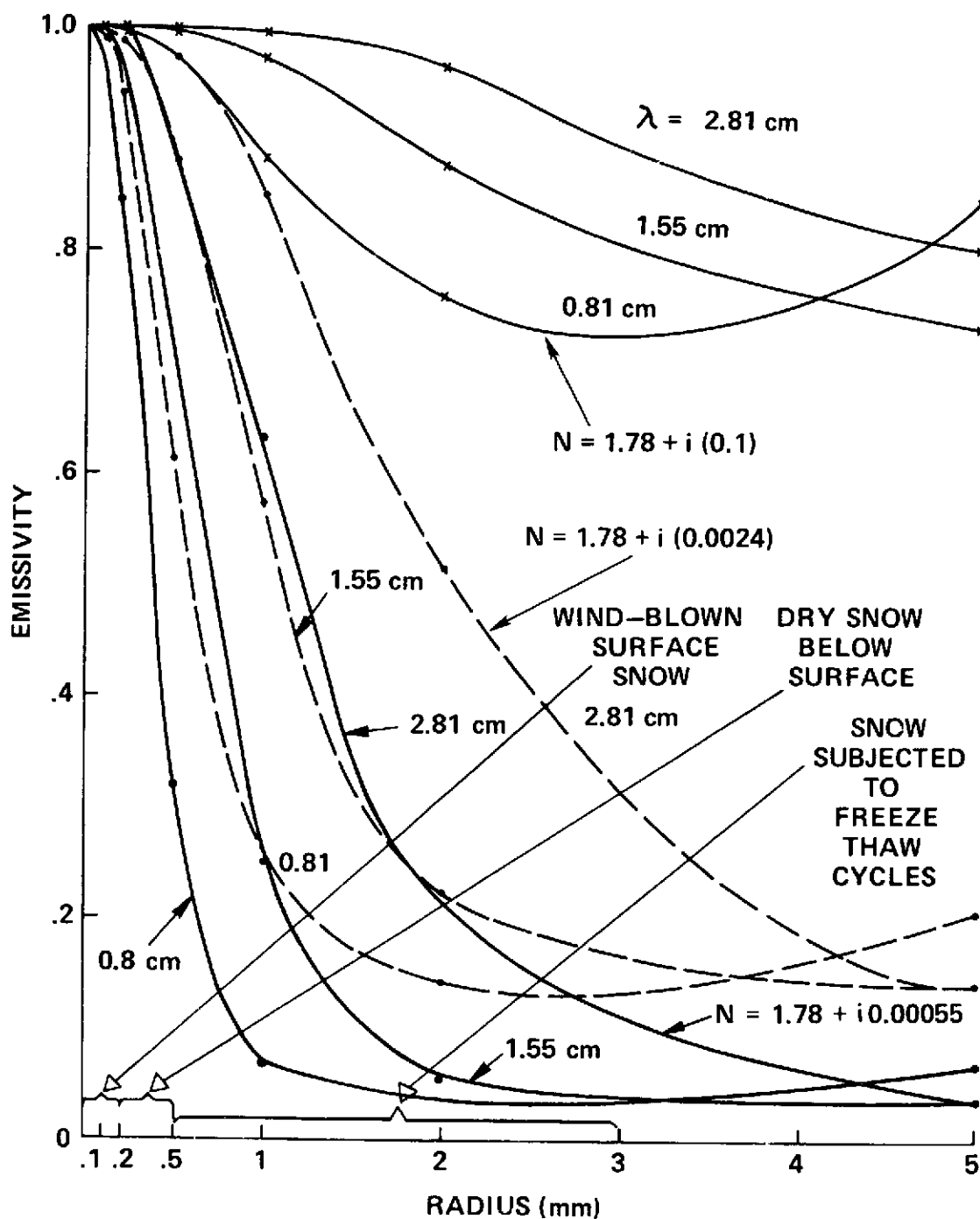
EMISSIVITY vs ICE CRYSTAL RADIUS

Figure 10. Emissivity as a function of ice crystal radius for three
different values of the imaginary part of the index of
refraction and for three different wavelengths

UNIT VOLUME DIFFERENTIAL SCATTERING CROSS SECTION
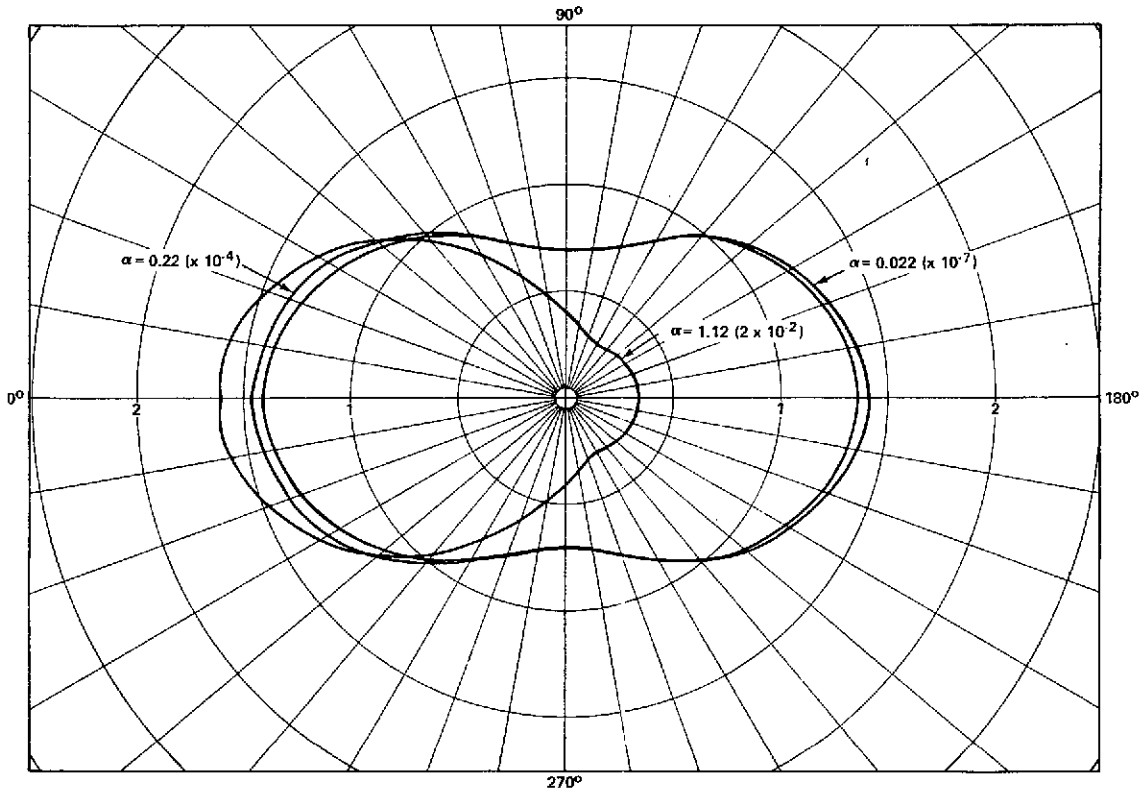
Figure 11. Unit volume differential scattering cross section for three
different values of the particle size parameter, α. The
quantities shown in parentheses are the scale factors to be
applied to the r-axis

IV. OBSERVATIONS AND DISCUSSION

An example of the spectral variation in the microwave emission of a snow-
covered temperate glacier is shown in Table 1. By neglecting the temperature
gradient in the snow, the simplified model calculations can be used to determine
the emissivity and consequently an average scattering particle diameter. The
emissivity is taken as the ratio of the brightness temperature to the physical
temperature of the surface, obtained both by remote measurements with an
airborne 10 micrometer radiometer and from surface reports (Schmugge et al,
1974). Assuming that the appropriate loss tangent for snow on a temperate
glacier is 0.0014 (Im(n) = 0.0024), the curves of Figure 10 were used to obtain
the particle radii listed also in Table 1. Note that the average radius increases

17

Table 1

Microwave Brightness Temperatures of the 8.4 m Snow Cover on
South Cascade Glacier (Station P-3, Elevation 2040 m, 1971 Data)

λ (cm)	T_B ($^\circ$K)	ϵ ($T_{physical}$ = 267 K)	ω_o	r(mm) (for $n\gamma$ = 0.0005)
0.81	206	0.77	0.7	0.15
1.55	194	0.72	0.8	0.5
2.81	224	0.84	0.6	0.5
6.01	238	0.88	0.5	1.0
11.	256	0.95	0.3	1-1.5

with the wavelength. Since the optical depth is greater for the longer wavelengths, the longer wavelength radiation is predominately from greater depths where the snow grain sizes are larger and the shorter wavelength radiation is from nearer the surface. These average radii are consistent with estimated grain sizes in the snow pack which range in radius from 0.15 mm near the top to 0.5 mm at the bottom (Meier 1974). Although the model calculations presented do not include the grain size, temperature, and density variations with depth, the simplified model does provide emissivities versus grain sizes which are consistent with the observations and at least qualitatively correct for wavelengths up to 2.81 cm. For the longer wavelengths, part of the radiation emanates from the glacier itself, and curves such as those in Figures 3-5 apply.

The computational results show that volume scattering from the individual grains is a dominant factor also in determining the emissivity of dry polar snow and firn, based on limited knowledge as to the particle sizes occurring in the snow cover. While this complicates the measurement of the near-surface temperature by microwave radiometry, it does provide a potential for measuring other parameters of glaciological interest, for example the extent of summer melting and snow accumulation rates.

As pure water ice nears the melting point, the loss tangent increases rapidly. In fact, for the thin liquid film that forms on the crystals, the loss tangent reaches a value the order of 0.4. Under these conditions, the scattering albedo, ω_o, is nearly zero (Figures 7-9) and the emissivity is nearly unity (Figure 6). This represents a plausible explanation of the sudden increase in

brightness temperature of snow observed near its melting point (Edgerton, et al, 1971; Gloersen et al, 1974). This effect should enable the mapping of the annual variations of the dry snow zones versus percolation or soaked zones in Greenland, for example.

A more detailed rationale is required to show the relation between snow accumulation rates and microwave brightness temperatures. It is known (Gow 1969, 1971) that the crystal size in dry firn is a function of time, t, and temperature, T,

$$D^2 = D_o^2 + k_o(e^{-E/RT})t \qquad (16)$$

where D^2 is the cross-sectional area at time t, D_o^2 is the initial cross-sectional area, k_o is a constant, E is the activation energy of the growth process per unit volume, and R is the gas constant. Also, the age, t, of a crystal at a particular depth, z, is a function of the snow load, σ, and the mean accumulation rate, A, i.e.,

$$t = \frac{\sigma(z)}{A} \qquad (17)$$

$\sigma(Z)$, which is the integral over the density versus depth curve also depends weakly on T and A. To illustrate that the dependence of $\sigma(z)$ on A can be neglected, a comparison of Maudheim (71.0° S, 10.8° W), where T = 256° K and A = 37 gm/cm², with Wilkes (66.1°S, 110.6° W, where T = 254° K and A = 13 gm/cm², indicates that the snow load at Z = 25 m differs by less than 10% while A differs by a factor of 3 (Gow 1968, 1969). Therefore, for a given temperature, the crystal size depth profile depends on the accumulation rate, which is the parameter of interest:

$$D^2(z) = D_o^2 + k_o(e^{-E/RT})\frac{\sigma(z)}{A} \qquad (18)$$

One must, of course, take into account the difference between crystals and grains, which are typically composed of one or two crystals (Gow 1969) and are a more likely measure of the scattering center size. However, grains and crystals have been observed to maintain a fairly constant mean size ratio of 1.4:1 (Gow, 1969).

In general, the gradient of $D^2(Z)$ increases with increased T or decreased A, as can be seen from equation (18). The dependence on A and T is clearly indicated in Figure 12, where crystal size profiles obtained at three different field measurement sites are illustrated.
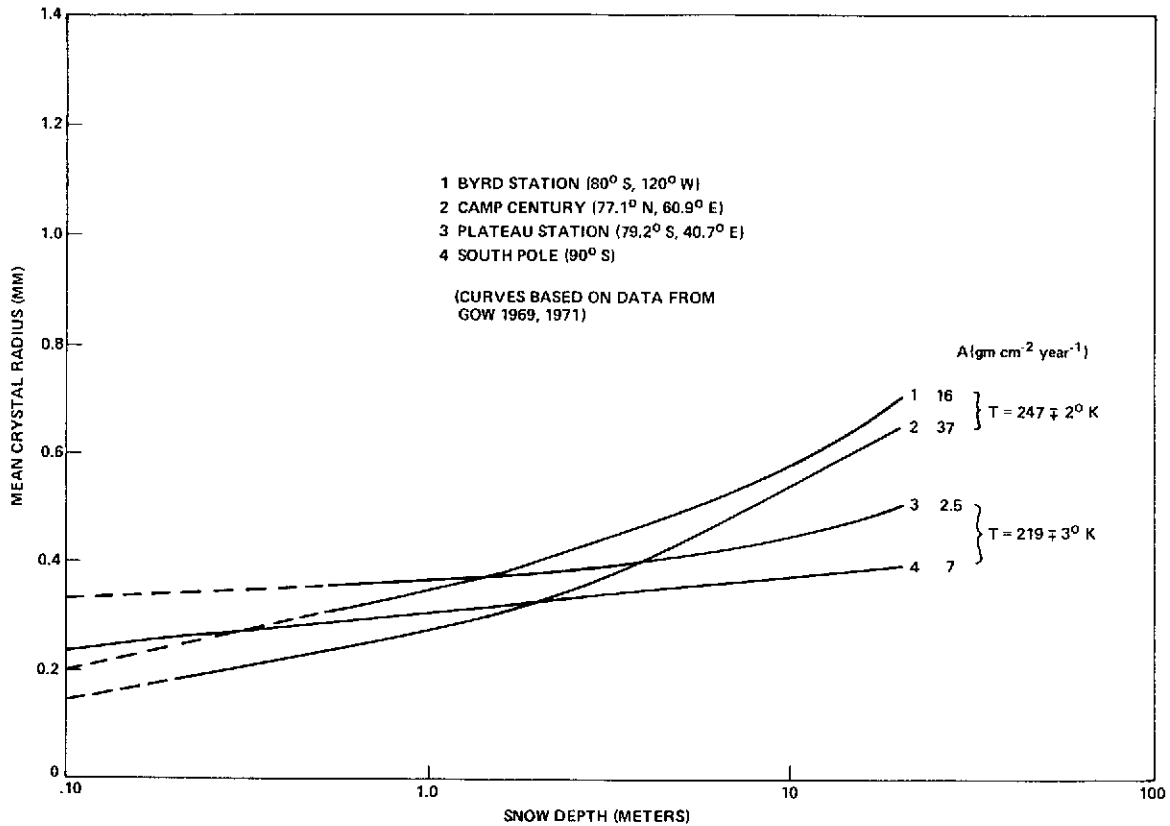
19

Figure 12. Ice crystal radius as a function of snow depth for several values of the accumulation rate, A and the average temperature, T. The values of the temperature are not shown with error limits; the minus refers to the smaller value of A and the + to the larger value. Note that the ice crystal radius variation with accumulation rate in each pair of curves bracketed runs counter to the trend that would be caused by temperature variation alone within that pair.

Now for the range of grain sizes encountered, the corresponding portions of the emissivity curves of Figure 10 can be approximated by:

$$\epsilon = 1 - \epsilon_o D^2 , \tag{19}$$

where $D^2 = \pi r^2$

20

Since the curves of Figure 10 were calculated on the basis of uniform particle sizes, it is necessary to replace D^2 in Equation (19) by $\overline{D^2}$, which is an average of Equation (18) over Z, weighted by the radiative transfer properties. As A increases, both D^2 (Equation (18)) and $\overline{D^2}$ will decrease and ϵ (Equation 19) will increase. Therefore, emissivity and accumulation rates should be directly correlated over areas of constant temperature.

We have in fact observed a remarkable correlation between the brightness temperature contours of the NIMBUS-5 ESMR (P. Gloersen et al., 1974) and the known accumulation rate patterns in Greenland (S. Mock, 1967) and Antarctica (C. Bull, 1971), despite the fact that the spatial variations of the physical temperature are included. Since a 10% variation in emissivity is roughly equivalent to a 25°K variation in temperature, it is not too surprising that emissivity variations dominate.

In order to make a more direct comparison between emissivity and accumulation rate patterns, an approximate emissivity has been obtained, i.e. the ratio of brightness temperatures obtained at the wavelengths of 1.55 cm and 10 micrometers. Such values cannot be obtained consistently because of persistent cloud cover, but were obtained on 11 January 1973 for Greenland (Figure 13) and Antarctica (Figure 14). Again, the areas with the highest emissivities are approximately those with the highest accumulation rates. In making these comparisons, it is necessary to consider regions with similar physical temperatures due to its effect on grain growth rate. In particular, the emissivity in Greenland (Figure 13) decreases from the central summit ($\epsilon = 0.85$) to the Northern region ($\epsilon = 0.70$) which has lower accumulation. It is approximately constant ($\epsilon = 0.75$) from Northwest of the summit toward Camp Century (see Figure 12) and increases from $\epsilon = 0.70$ on the low accumulation area on the Southwest to $\epsilon = 0.85$ on the very high accumulation area on the Southeast. In Antarctica (Figure 14), the emissivity is low ($\epsilon = 0.70$) over the low accumulation central East Antarctica plateau (vicinity of 80°S, 90°E). It is high ($\epsilon = 0.85$) in the high accumulation area at the base of the Antarctic peninsula in contrast to a low value ($\epsilon = 0.70$ to 0.75) in the Ross Ice Shelf drainage basin part of West Antarctica (vicinity of 82°S, 140°W). In both Southern Greenland and the Byrd station region of West Antarctica (80°S, 120°W), the T_B contours are parallel to the ice divides which also mark regions of differing accumulation rates.

In the case of the Lambert Glacier (72°S, 68°W) in Antarctica, the emissivity is also high, about 0.85. It is known (W. Budd, 1974) that this glacier has extended areas of exposed blue ice due to vigorous wind action in the area; such areas would be expected on the basis of this model to have very low scattering albedo and hence high emissivity (see Figure 6). Thus, a high emissivity does not necessarily imply a high snow accumulation rate over a glacier. Therefore, some prior knowledge of the general characteristics of the snow field is required to interpret properly the observed brightness temperatures.
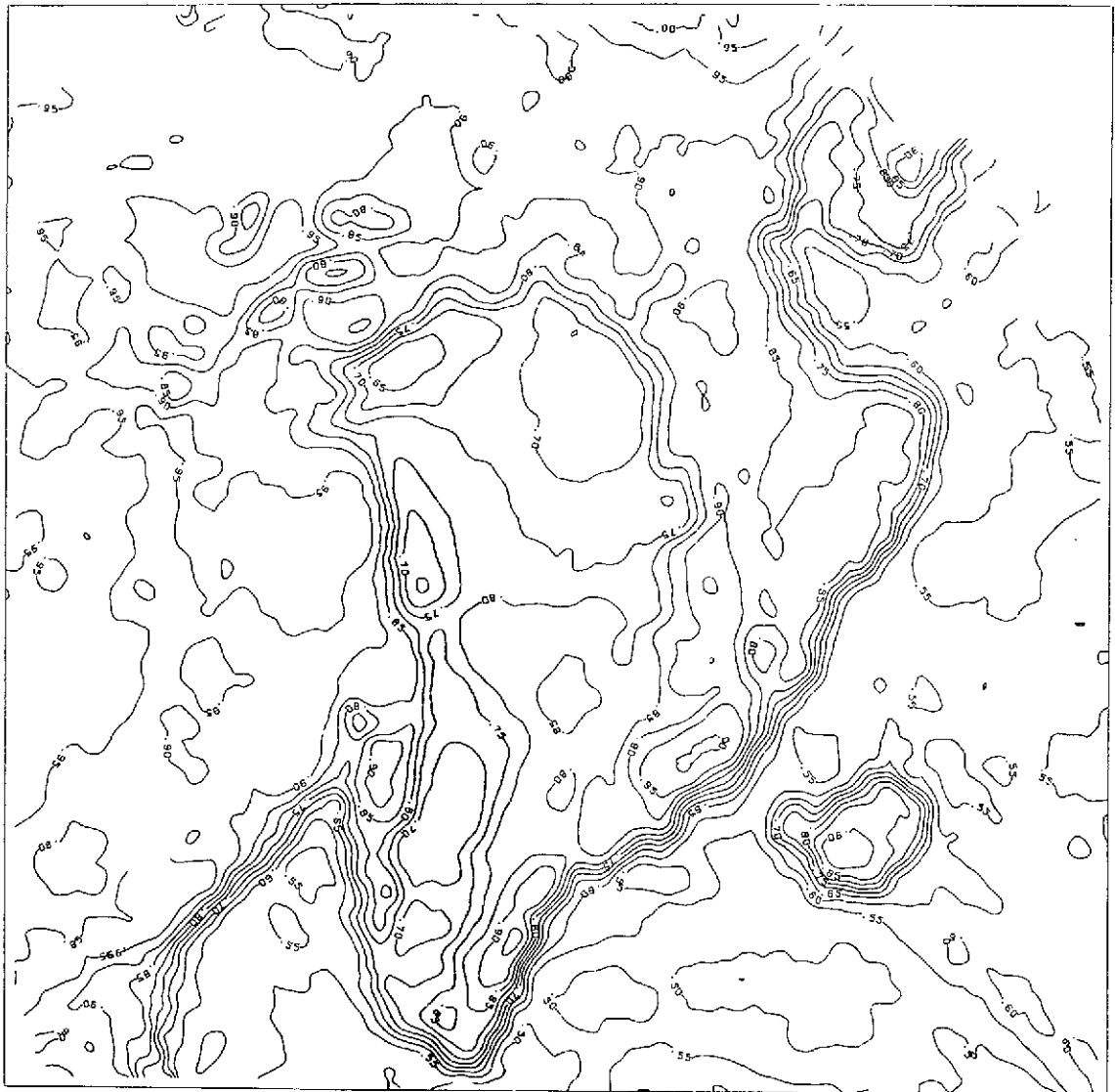
EMISSIVITY CONTOURS ON GREENLAND
1 /11/73

Figure 13. Contours of constant emissivity at a microwave wavelength of 1.55 cm on Greenland. The emissivity values were obtained by taking the ratio of the brightness temperatures obtained at wavelengths of 1.55 cm to those obtained at wavelengths of 10 micrometers from instruments on board the NIMBUS-5 satellite. The data were obtained on a relatively cloud-free day (Jan 11, 1973).

22
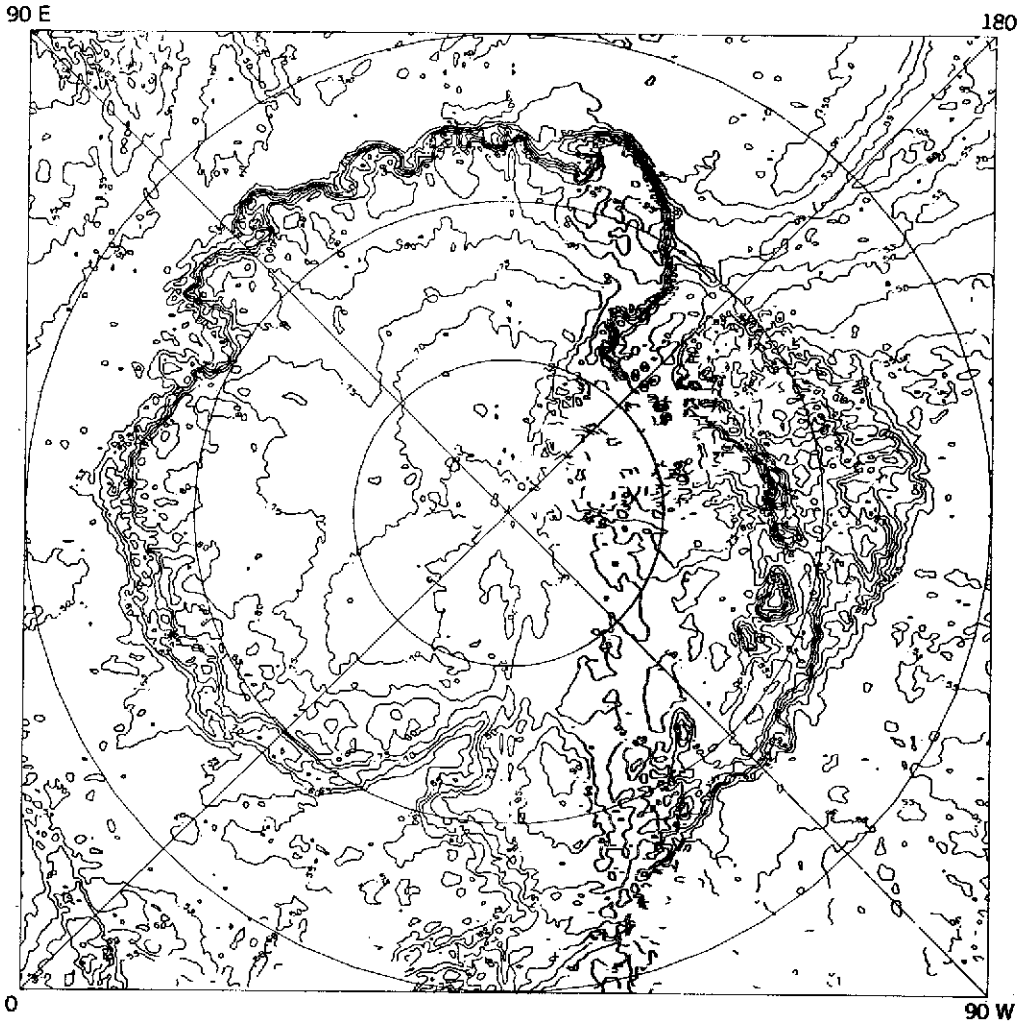
EMISSIVITY CONTOURS ON THE ANTARCTIC CONTINENT
1/11/73

Figure 14. Contours of constant emissivity at a microwave wavelength of
1.55 cm on Antarctica. The emissivity values were obtained by
taking the ratio of the brightness temperatures obtained at wave-
lengths of 1.55 cm to those obtained at wavelengths of 10 micro-
meters from instruments on board the NIMBUS-5 satellite. The
data were obtained on a relatively cloud-free day (Jan 11, 1973).

V. CONCLUSIONS

A microscopic model, which considers the individual snow grains as the scattering centers and employs Mie extinction and scattering coefficients, has been used to obtain a qualitative explanation of the low brightness temperatures observed over snow fields and snow-covered glaciers. More quantitative descriptions will be provided by this model when the vertical grain size distribution, physical temperature, and variation in loss tangent are taken into account. The present work has given essentially the same results as England (1974) in terms of the variation of brightness temperature with the scattering albedo ω_0. The results differ in detail, however, because England assumed isotropic scattering in his model; Mie scattering, assumed here, is anisotropic. An additional result of the present analysis is the determination of the variation of ω_0 as a function of particle sizes, wavelength, and loss tangent. It has been shown that in the wavelength range from 0.8 to 2.8 cm, and for snow crystal sizes normally encountered, most of the microwave radiation emanates from a layer the order of 10 meters or less in thickness. An additional important result of this analysis is the explanation of the wet snow signature in terms of a wet surface on the snow crystals and the resulting sudden increase in the loss tangent of the scatterers which, in turn, gives rise to near-zero values for ω_0, the scattering albedo. Finally, it is concluded that it may be possible to determine snow accumulation rates as well as near-surface temperatures by utilizing this model in conjunction with multispectral observations in the microwave region.

REFERENCES

Budd, W., Private Communication (1974)

Bull, C., "Snow Accumulation in Antarctica," Research in Antarctica, American Association for Advancement of Science (1971)

Chandrassekhar, S., "Radiative transfer," Claredon, Oxford (1950)

Cumming, W. A., "The dielectric properties of ice and snow at 3.2 cm," J. Appl. Phys. 23, 768 (1952)

Curran, R. J., B. J. Conrath, H. L. Kyle, and W. C. Meyer, "Infrared radiation transfer calculations for clouds and comparison with satellite observations," manuscript in preparation (1975)

Edgerton, A. T., A. Stogryn and G. Poe, 1971. Microwave radiometric investigations of snowpack. Final report no. 1285 R-4 for U.S.G.S.

24

contract no. 14-08-001-11828, Aerojet-General Corp., Microwave Division, El Monte, California

England, A. W., "Thermal microwave emission from a halfspace containing scatterers," Radio Science 9, 447 (1974)

Gaut, N. E., and E. C. Reifenstein, III, "Interaction model of microwave energy and atmospheric variables," NASA Contract Report CR-61348 (1971)

Gloersen, P., T. T. Wilheit, T. C. Chang, W. Nordberg, and W. J. Campbell, "Microwave maps of the polar ice of the earth," Bul. Am. Met. Soc. 12, 1442 (1974)

Gow, A. J., "Deep Core Studies of the Accumulation and Densification of Snow at Byrd Station and Little America V, Antarctica," U.S. Army CRREL Research Report 197 (1968)

Gow, A. J., "On the Rates of Growth of Grains and Crystals in South Polar Firn," Journal of Glaciology Vol 8, No. 53 (1969)

Gow, A. J., "Depth-time-temperature Relationships of Ice Crystal Growth in Polar Regions," U. S. Army CRREL Research Report 300 (1971)

Hoekstra, P. and P. Cappillino, "Dielectric properties of sea and sodium chloride ice at UHF and microwave frequencies," J. Geoph. Res. 76, 4922 (1971)

Hildebrand, F. B., "Introduction to numerical analysis," Chapter 10, McGraw-Hill, New York (1956)

Meier, M. F., Private Communication (1974)

Mie, G., Ann. Phys. 25, 377 (1908)

Mock, S., "Accumulation Patterns on the Greenland Ice Sheet," U. S. Army CRREL Research Report 233 (1967)

Schmugge, T., T. T. Wilheit, P. Gloersen, M. F. Meier, D. Frank, I. Dirmhirn, "Microwave Signatures of Snow and Fresh Water Ice," in Study of Snow and Ice Resources, pp 551-562, National Academy of Sciences, Washington, D. C. (1974)

Stratton, J. A., "Electromagnetic theory," pp 563-573, McGraw-Hill, New York (1941)